Journal of Archaeology and Archaeometry. December,2025, VOL.4.NO.3(15)1-13.

Journal of Archaeology and Archaeometry

/h t t p s : / / s a n a d . i a u . i r / j o u r n a l / j a a

Original Article

New Insights into Early Islamic Glass from Jorjan by Archaeometric Investigation Using LIBS and SEM-EDXS

Farahnaz Bayat Nejad[1]* Mohammadamin Emami[2] Mohammad Eghbal Chehri[3] Maryam Kolbadinejad[4] Rémy Chapoulie[5]

[1]Department of History and Archaeology, CT.C. Islamic Azad University, Tehran, Iran
[2]Department of Conservation of Cultural Properties and Archaeometry, Art University of Isfahan, Isfahan, Iran
[3]Department of History and Archaeology, CT.C. Islamic Azad University, Tehran, Iran
[4]Department of History and Archaeology, CT.C. Islamic Azad University, Tehran, Iran
[5]CNRS, University Bordeaux Montaigne, Bordeaux, France 6034 Archéosciences Bordeaux / UMR

Publisher: Islamic Azad University of Varamin-Pishva Branch

Article Info

Article History:
Recived: 2025/10/07
Revised: 2025/10/20
Accepted: 2025/11/20
AvailableOnline: 2025/12/30

KeyWords:
Jorjan
Archaeology
Archaeometry
Glass
Early Islamic Glass
LIBS; SEM-EDX
Silk Road

*Corresponding author:
E-mail address:

aminemami.ae@gmail.com

Abstract

This study presents the analysis of nineteen glass samples from Jorjan (northeastern Iran), dating to the Early Islamic period, using Laser-Induced Breakdown Spectroscopy (LIBS) as a first approach. While LIBS allowed rapid screening of elemental patterns, its quantification is not yet fully mastered; therefore, complementary SEM–EDXS analyses were performed for comparative purposes and validation of the results. Both methods consistently show strong calcium (Ca) and potassium (K) with variable sodium (Na), indicating the dominance of plant-ash flux technology and aligning with the well-known transition from natron to plant ash in the 8th–9th centuries CE. Variability in Na (and minor Al) intensities points to multi-source raw materials and highlights Jorjan's role in regional production and exchange along the Silk Road. We also provide an integrated spectral comparison, group the assemblage by Na and Ca peak strengths, and discuss the analytical and heritage-conservation advantages of LIBS—when supported by SEM–EDXS—for the study of archaeological glass.

Citation:Bayatnejad, F.Emami,M.A. Eghbal CHehri. M. Kolbadinejad, M. Chapoulie, R. (2025). New Insights into Early Islamic Glass from Jorjan by archaeometric Investigation Using LIBS and SEM-EDXS. Journal of Archaeology and Archaeometry, 4(3).1-13.

Doi: https://doi.org/10.71647/Jaa.2025.1220430 e-ISSN: 2821_1928

Introduction

Jorjan (present-day town of Gorgan) was a major cultural and commercial hub in northeastern Iran. Archaeological research over the past century—ranging from early surveys by Vandenberg and Jacques de Morgan to systematic excavations—has revealed extensive urban remains and craft traditions, including glassmaking. Studying Jorjan's glass provides insight into technological choices, raw-material procurement, and exchange networks along the Iranian Silk Road. For geographical contextualization, a locator map showing Jorjan's position along the Silk Road is shown in Figures 1 and 2. Laser-Induced Breakdown Spectroscopy (LIBS) is a rapid, minimally destructive technique increasingly used in archaeometry. A pulsed laser generates a micro-plasma on the sample; emitted light is dispersed and recorded to identify elemental lines. For ancient glass, LIBS can distinguish flux types (natron vs. plant ash), detect stabilizers (lime), and screen minor/trace oxides, offering significant benefits when sampling is constrained (Detalle et al. 2022). Methodologically, LIBS provides a rapid, minimally destructive screen to identify diagnostic lines (e.g., Ca II 393.3/396.8 nm, Na I 589.0/589.6 nm, K I 766.5/769.9 nm) and to compare relative intensities across specimens when sampling for calibration-based quantification is constrained (De Sá et al., 2011; Van der Sloot et al., 2007; Botto et al. 2019). Line assignments were checked against standard compilations (NIST Atomic Spectra Database). While LIBS excels at qualitative grouping and peak-based screening, quantitative provenance and robust modeling ultimately require calibrated methods (e.g., SEM–EDS, LA–ICP–MS) (May et al., 2016; De Sá et al., 2011). Within this framework, Jorjan (Gorgan) offers a key vantage point to assess raw-material procurement, workshop practice, and exchange. If plant-ash fluxes dominate, one expects strong Ca and K with variable Na intensities; conversely, natron glass tends to show conspicuously higher and more uniform Na with lower K. Stabilization is primarily provided by CaO (lime), often introduced via calcareous sands or the plant ash itself (Freestone, 2006). By sampling morphologically and chromatically diverse fragments (body, base, handle, neck/rim; greens, yellows, blues, purples, browns, olive-green), the present study is designed to capture recipe variability and assess whether secondary working correlates with subtle compositional differences. From a technological perspective, Early Islamic glassmaking in Iran sits at the hinge between late Roman–Byzantine traditions reliant on mineral natron and the widespread adoption of plant-ash fluxes. In the Levant and Egypt, natron (a naturally occurring soda source) underpinned large-scale primary production through Late Antiquity; its decline and eventual substitution by plant ash are now well documented in both archaeological and compositional datasets (Freestone, 2006; Shortland, 2004; Phelps et al., 2016). In Iran, assemblages along the Silk Road reveal regional adaptations of this transition, with halophytic plant ashes supplying K- and Ca-bearing fluxes in lieu of natron-derived soda (Schibille et al., 2018).

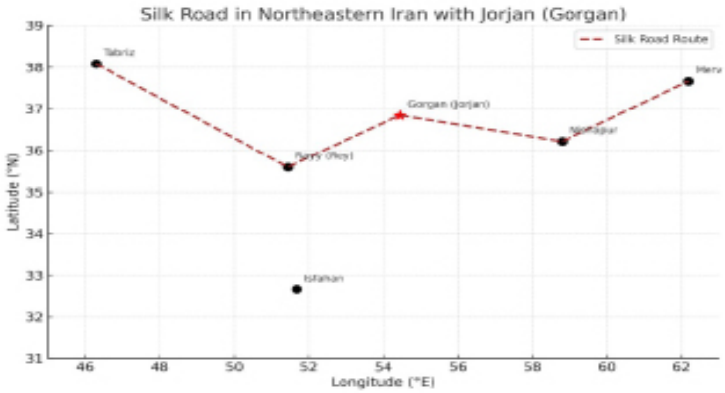

Figure1.
Locator map showing the position of Jorjan (modern Gorgan) in northeastern Iran and along the Silk Road routes. The Great Wall of Gorgan alignment and UNESCO-listed Gonbad-e Qābus tower are also indicated. Coordinates in WGS84.

Figure2.
Map of the Silk Road during the Late Sasanian and Early Islamic periods, showing major nodes including Jorjan (Gorgan), Rey, Istakhr, Bukhara, Antioch, and Aleppo. The location of Jorjan highlights its strategic position within the Iranian Plateau and its role as a hub for technological and cultural exchange along the eastern trade routes.

Materials and Methods

Nineteen archaeological glass fragments (J1–J19 in Figure 3) were deliberately selected to capture maximum technological and visual variability. Specimens originate from distinct vessel zones—body sherds, bases, handles, and neck/rim fragments—and span a wide color gamut (green to olive-green, yellow/amber, blue, purple/violet, and brown) with varying thickness/curvature. This breadth supports inter-sample comparison and the assessment of recipe diversity (balance of Ca–K–Na and minor oxides).

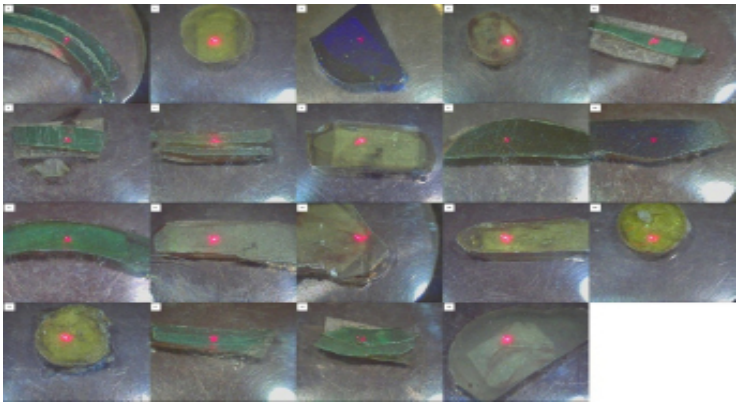

Figure3.
Macroscopic photographs of selected Jorjan glass fragments (J1–J19) showing LIBS analysis spots (red dots). Diagnostic emission lines of Cu (324, 510 nm), Ca (393.3 nm), Na (589.0 nm), and K (769.5 nm) are indicated by vertical dashed lines. Scale bar = 5 mm.

Sample Preparation and Measurement Protocol

Prior to analysis, each specimen was cut and carefully polished to obtain a flat, mirror-finish cross-section. To avoid weathering skins or adherent deposits, all LIBS spots were placed on the freshly exposed interior ("core") glass, deliberately away from the original external surface, cracks, bubbles, and visible inclusions. Probed areas were screened under a binocular microscope and selected only if free of visible contamination, weathering, or surface damage. Measurements were acquired under consistent conditions across all samples, with spots placed on visually homogeneous domains to ensure comparability.

Instrumentation LIBS and SEM-EDXS

Analyses were performed at Archéosciences Bordeaux (Université Bordeaux Montaigne) using an IVEA LIBS system (class 4 laser, 1064 nm, 40 mJ, 1 Hz; focal distance ≈10 cm). Elemental identifications reference standard line lists including the NIST Atomic Spectra Database. Complementary compositional analyses were performed by SEM–EDXS Archéosciences Bordeaux (Université Bordeaux Montaigne). Analyses employed a JEOL IT-500HR Field Emission Gun (FEG) scanning electron microscope operated at 20 kV in Low Vacuum mode (30 Pa). Two Oxford Instruments UltimMax 100 mm² SSD detectors were attached, with acquisition controlled by the AZtec software suite. Cross-sections of glass fragments (J1–J19) were polished and analyzed on fresh fracture surfaces. Analyses targeted homogeneous glassy matrix domains, avoiding weathered surfaces, cracks, and inclusions. Multiple points (1–8 per specimen) were acquired, and data were corrected by ZAF procedures. Results are reported as oxide wt% (mean ± 1σ, with n = number of valid points retained).

Results

Across J1–J19 (Figures 4 to 10), diagnostic Ca II (393.3/396.8 nm), K I (766.5/769.9 nm), and Na I (589.0/589.6 nm) lines are present, with Ca and K generally dominant and Na varying from weak to strong. To visualize these patterns, we compiled: (i) an overlay of all spectra, (ii) Na-based groups (Na-poor, Na-moderate, Na-rich), (iii) Ca-based groups (tertiles of the Ca II 393–397 nm peak), and (iv) a peak-identification graph annotating canonical lines.

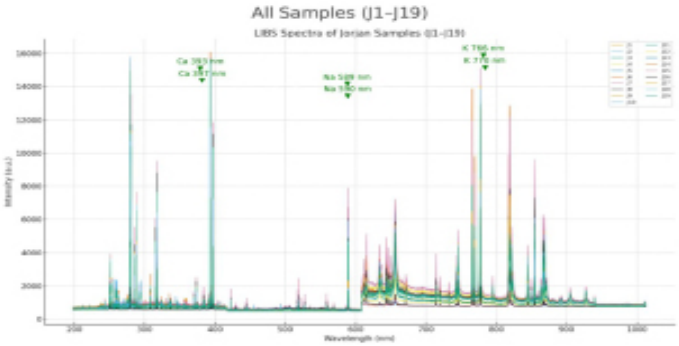

Figure4.
Overlay of LIBS spectra for all samples (J1–J19).

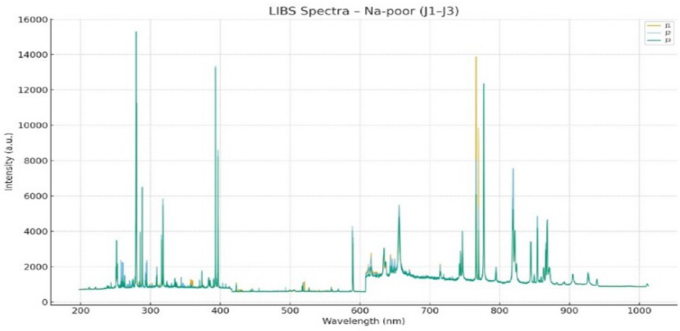

Figure5.
Na-poor group (J1–J3).

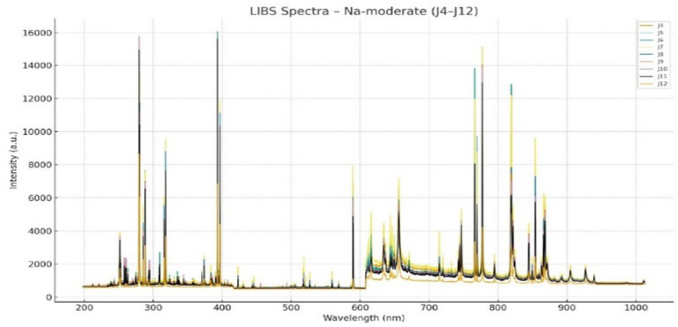

Figure6.
Na-moderate group (J4–J12).

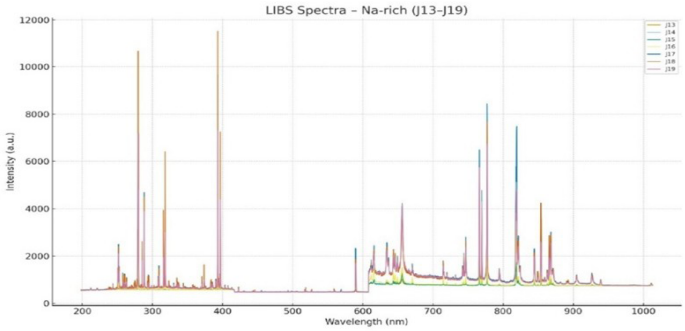

Figure7.
Na-rich group (J13–J19).

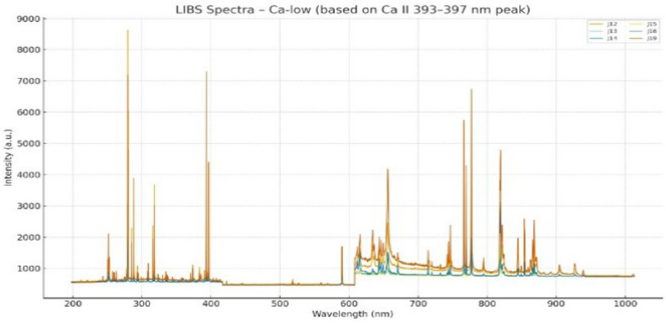

Figure8.
Ca-low group (tertile based on Ca II 393–397 nm).

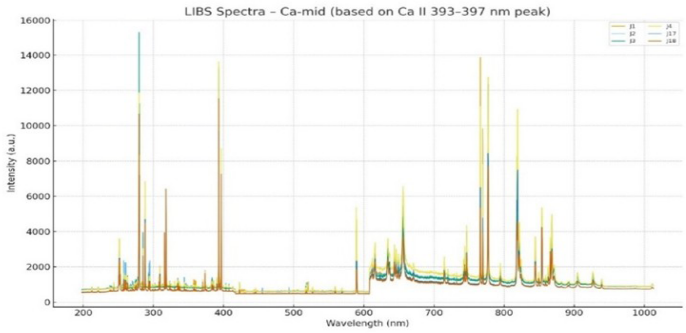

Figure9.
Ca-mid group (tertile based on Ca II 393–397 nm).

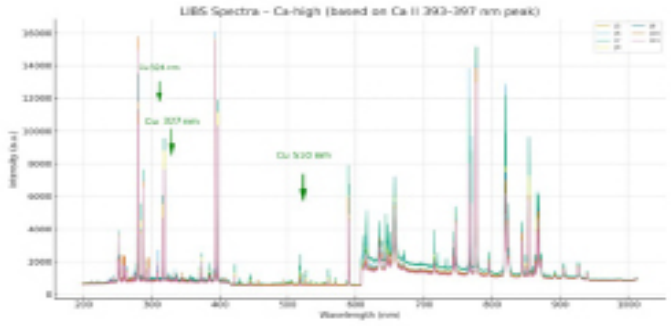

Figure10.
Ca-high group (tertile based on Ca II 393–397 nm) LIBS spectra of selected green-blue fragments, showing Cu emission lines (e.g., 324, 327, 510 nm), consistent with deliberate coloring."

Figure11.
Peak-identification map with canonical lines (Si, Ca, Al, Sr, Na, K)

The diagrams reveal consistent silicium (Si) dominance, accompanied by significant Ca and K signals, confirming plant ash as the primary flux. Variations in Na intensity are diagnostic: samples J3, J8, and J14 exhibit elevated sodium peaks, possibly from recipe differences or sodium-rich sands. Samples J5, J11, and J19 show higher Sr and Ba, linked to local sands or plants, thus serving as geochemical fingerprints. Clustering in Ca vs. K plots indicates at least two compositional traditions—one Ca-rich, one K-dominated—suggesting flexible practices or multiple raw sources. Sample-by-sample narratives (J1–J19) corroborate these trends. In brief: J1–J3 show strong Ca and K with weak/absent Na; J4–J12 retain strong Ca and K with clearly present Na; J13–J19 display comparatively higher Na contributions. All samples confirm a silica-based matrix with Al variably present (sand- or plant-derived).

Table1.
Calcium (Ca II, 393–397 nm) LIBS peak positions and intensities for Jorjan samples.

Sample	Ca peak position (nm)	Ca relative intensity (arbitrary unit)
J1	393	13182
J2	393	13343
J3	393	13227
J4	393	13607
J5	393	14726
J6	393	16064
J7	393	15691
J8	393	15685
J9	393	15260
J10	393	15671
J11	393	15610
J12	393	0853
J13	393	1101
J14	393	1854
J15	393	188
J16	393	3092
J17	393	9678
J18	393	11529
J19	393	7298

Table 2 summarizes the relative LIBS peak positions and intensities of sodium (Na I, 588.9–589.7 nm). These values, while qualitative, provide insight into the degree of Na contribution to the glass network as a flux modifier. They form the basis for grouping the samples into Na-poor, Na-moderate, and Na-rich categories, reflecting variability in raw materials and recipe choices. Fluctuations in Na intensity may indicate different plant-ash sources, preparation techniques, or incidental inputs from sodium-rich sands. Intensities should therefore be interpreted comparatively rather than as absolute concentrations.

Table2.
Sodium (Na I, 588.9–589.7 nm) peak positions and intensities (J1–J19).

Sample	Na_peak_position (nm)	Na_ relative intensity (arbitrary unit)
J1	589	4113
J2	589	4281
J3	589	4007
J4	589	5364
J5	589	7121
J6	589	6218
J7	589	7898
J8	589	6033
J9	589	5296
J10	589	5917
J11	589	4868
J12	589	1093
J13	589	594
J14	589	608
J15	589	778
J16	589	865
J17	589	2337
J18	589	1856
J19	589	1704

Table 3 presents the LIBS peak positions and relative intensities for potassium (K I, 766.5/769.9 nm). Potassium is a primary flux component in plant-ash glass, and variations in its intensity highlight differences in halophytic plant sources and ash processing. Together with Ca II, the K I intensities help distinguish Ca-rich versus K-dominated compositional traditions, providing a framework for discriminating workshop practices and raw material supply strategies. As with sodium, these intensities are comparative indicators and are supplemented with a calibrated method (SEM–EDXS) for precise quantification.

Table3.
Potassium (K I) peak positions and intensities (J1–J19).

Sample	K766 peak_nm	K766 intensity	K770 peak_nm	K770 intensity	K max peak_nm	K max intensity
J1	766	1386	769	9835	766	13868
J2	766	8044	769	5426	766	8044
J3	766	6075	769	408	766	6075
J4	766	11093	769	7804	766	11093
J5	766	9834	769	6768	766	9834
J6	766	13832	769	9725	766	13832
J7	766	11959	769	8787	766	11959
J8	766	6531	769	4585	766	6531
J9	766	7886	769	5447	766	7886
J10	766	7479	769	5141	766	747
J11	766	8059	769	5587	766	8059
J12	766	3349	769	2630	766	3349
J13	766	1462	769	1309	766	1462
J14	766	1727	769	1473	766	1727
J15	766	2206	769	1818	766	2206
J16	766	3885	769	3047	766	3885
J17	766	6488	769	4772	766	6488
J18	766	5341	769	3910	766	5341
J19	766	5739	769	4296	766	5739

Table 1 lists the relative LIBS peak positions and intensities for calcium (Ca II, 393–397 nm). Calcium acts as a stabilizer (lime, CaO), commonly introduced via calcareous sands or plant ash. Variations in Ca intensity highlight differences in raw material input and recipe stability. These values, though qualitative, allow identification of Ca-rich versus Ca-poor samples and serve as a baseline for distinguishing technological choices and workshop practices. Intensities should be read comparatively rather than as absolute concentrations.

LIBS relative intensities are presented to highlight comparative elemental patterns across samples. These values serve to identify enrichment/depletion trends, major glass-forming oxides, potential flux sources, and trace fingerprints for workshop discrimination

Integrating LIBS and SEM–EDXS data

The LIBS screening identified the major compositional framework dominated by Ca, K, Na, Si, and Al. SEM–EDS quantification confirms these observations and provides calibrated oxide data. Table 4 presents the average compositions (mean ± SD, wt%) per specimen.

Table4.
SEM–EDXS oxide compositions of Jorjan glass samples (wt%, mean ± SD; n = number of points).

J6	135.62 ± 0.24 (n=3)	22.41 ± 0.10 (n=3)	4.86 ± 0.01 (n=3)	7.12 ± 0.03 (n=3)	4.47 ± 0.09 (n=3)	7.48 ± 0.05 (n=3)	1.97 ± 0.01 (n=3)	1.86 ± 0.02 (n=3)	0.34 ± 0.01 (n=3)	0.81 ± 0.05 (n=3)	0.00 ± 0.00 (n=3)	0.00 ± 0.00 (n=3)	0.00 ± 0.00 (n=3)	1.00 ± 0.02 (n=3)
J7	142.64 ± 0.11 (n=3)	20.14 ± 0.20 (n=3)	3.39 ± 0.01 (n=3)	7.62 ± 0.06 (n=3)	7.66 ± 0.03 (n=3)	4.42 ± 0.12 (n=3)	1.01 ± 0.01 (n=3)	1.62 ± 0.02 (n=3)	0.21 ± 0.02 (n=3)	0.32 ± 0.05 (n=3)	0.00 ± 0.00 (n=3)	0.00 ± 0.00 (n=3)	0.00 ± 0.00 (n=3)	0.71 ± 0.03 (n=3)
J8	138.48 ± 0.39 (n=3)	24.88 ± 0.21 (n=3)	2.67 ± 0.01 (n=3)	8.22 ± 0.06 (n=3)	6.13 ± 0.03 (n=3)	3.76 ± 0.11 (n=3)	1.11 ± 0.01 (n=3)	1.12 ± 0.01 (n=3)	0.14 ± 0.02 (n=3)	0.33 ± 0.03 (n=3)	0.00 ± 0.00 (n=3)	0.00 ± 0.00 (n=3)	0.00 ± 0.00 (n=3)	0.69 ± 0.04 (n=3)
J9	135.53 ± 0.43 (n=3)	22.40 ± 0.31 (n=3)	3.43 ± 0.05 (n=3)	7.40 ± 0.23 (n=3)	5.17 ± 0.12 (n=3)	6.66 ± 0.13 (n=3)	3.57 ± 0.44 (n=3)	1.27 ± 0.11 (n=3)	0.39 ± 0.03 (n=3)	0.91 ± 0.05 (n=3)	0.00 ± 0.00 (n=3)	0.00 ± 0.00 (n=3)	0.00 ± 0.00 (n=3)	0.99 ± 0.12 (n=3)

Key diagrams (Figures 11 to 14) highlight technological and raw material implications.

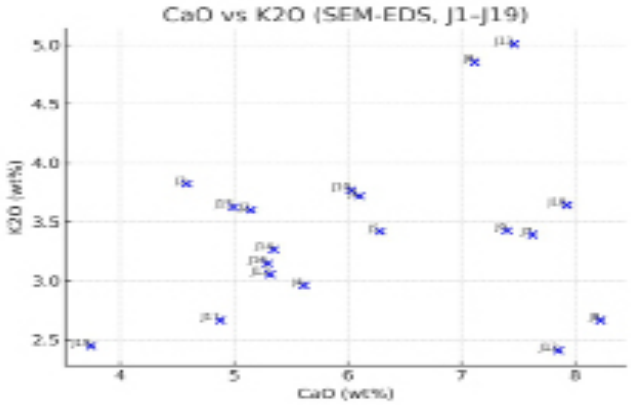

Figure12.
CaO vs K2O (wt%). Bivariate distribution highlighting Ca-rich and K-rich glassmaking recipes within the Jorjan assemblage

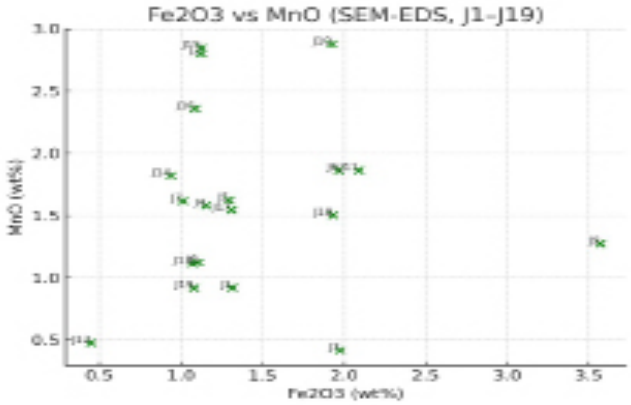

Figure13.
Fe2O3 vs MnO (wt%). Colorant-related oxides reflecting the roles of Fe as chromophore and Mn as decolorant.

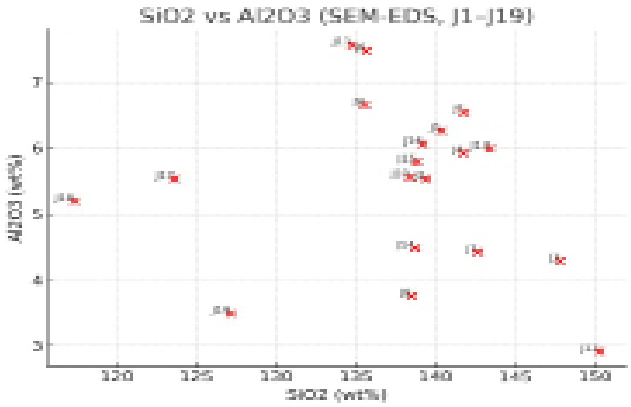

Figure14.
SiO2 vs Al2O3 (wt%). Positive correlation suggests alumina contributions from alumino-silicate sands.

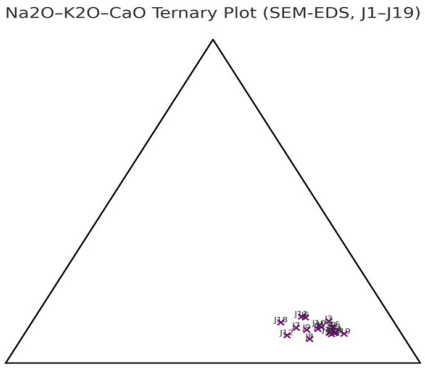

Figure15.
Na2O–K2O–CaO ternary diagram. Samples cluster in the plant-ash compositional field, distinguishing them from natron-type glass.

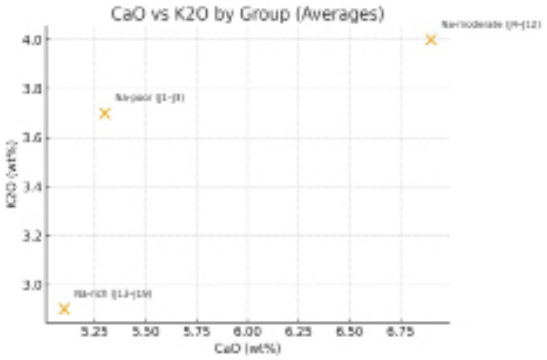

Figure16.
Scatterplot of group-averaged CaO and K2O (wt%). Labels indicate Na-based groups (Na-poor, Na-moderate, Na-rich).

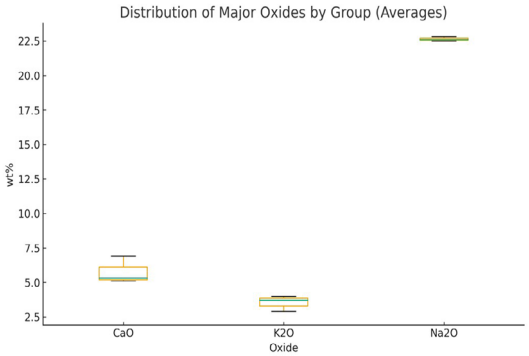

Figure17.
Distribution of Major Oxides by Group (Averages).

Boxplot of Na2O, K2O, and CaO (wt%) averages across groups, showing structured variability in recipes (Figures 15 and 16). As summarized in the Discussion (see Figure 15 and Figure 16), the Ca–K balance and Na variability define two recurrent recipes and structured inter-group differences.

Discussion

Technological implications

The Jorjan assemblage is compositionally consistent with plant-ash glassmaking, showing dominant Ca and K with variably expressed Na, as evidenced by canonical LIBS lines (Ca II 393.3/396.8 nm; Na I 589.0/589.6 nm; K I 766.5/769.9 nm) and corroborated by SEM–EDXS oxides (Table 4). Grouping by Na intensity (Na-poor J1–J3; Na-moderate J4–J12; Na-rich J13–J19) reveals structured variability that likely reflects differences in halophytic plant ashes, ash preparation, and incidental inputs from sodium-bearing sands. The CaO–K2O scatter clarifies two recurrent recipes—Ca-rich versus K-rich (Figure X)—while the Na2O–K2O–CaO ternary places all samples firmly within the plant-ash field and away from natron-type glass (Figure 15). Together, these patterns indicate flexible workshop practice rather than a single standardized tradition (Oujja et al. 2021).

Compositional structure and clustering

The integrated datasets show that while Na2O spans a relatively broad range, the CaO–K2O balance is more diagnostic for discriminating subgroups. Samples J6–J10 plot toward the Ca-rich edge, whereas J1–J3 are K-dominated (Figure 1). The boxplot of group averages (Figure 16) visually summarizes between-group contrasts, complementing the overlay and subgroup spectral figures (Figures 4–11). Interpreting LIBS peak intensities as comparative (semi-quantitative) is critical: minor mismatches between LIBS intensities and SEM–EDXS wt% are expected due to matrix effects and plasma–sample coupling, hence the need for calibrated methods alongside screening.

Trace oxides and provenance potential

Selective enrichments in Sr and Ba (notably in J5, J11, J19) suggest variability in raw sands and/or plant sources and provide a provenance-sensitive fingerprint worth pursuing with targeted comparisons (e.g., Sr-isotope frameworks) in future work. Within the present dataset, these enrichments co-occur with the Ca-rich subgrouping, consistent with contributions from calcareous sands and certain halophyte ashes observed in Early Islamic traditions. While the current evidence is preliminary, the co-variation of Ca with Sr (and to a lesser degree Ba) supports the interpretation that raw-material procurement was multi-source, potentially mixing sands of differing geologies.

Colorants and chromatic control

The assemblage exhibits Fe-controlled amber/brown hues and Mn as decolorant/chromophore, in line with regional practices; traces of Cu detected by LIBS in select green-blue fragments indicate deliberate coloring (Figure 11).(Traces of Cu detected by LIBS in select green-blue fragments indicate deliberate coloring (Fig. 10)). SEM–EDS Fe2O3 and MnO distributions align with visual classifications and reinforce the role of redox and additive control during secondary working and finishing. This chromatic palette is consistent with contemporaneous Early Islamic workshops and supports the view that color was technologically and aesthetically managed rather than incidental.

Regional context and comparisons

Within the broader natron-to–plant-ash transition of the 8th–9th centuries CE, the internal heterogeneity at Jorjan parallels patterns reported from Rayy, Istakhr, and Bukhara: all indicate multiple raw-material sources and adaptive recipes within connected exchange networks. The Jorjan data fit this picture—plant-ash dominance with variable Na, K, and Ca; Ca- vs. K-rich pathways; and trace-oxide signatures indicative of diverse sands—supporting the interpretation of Jorjan as both a local production locus and a Silk Road node for distribution.

Methodological reflections and future directions

LIBS provided rapid, micro-destructive screening and grouping, but intensities remain semi-quantitative; SEM–EDXS added calibrated oxide data and made visible low-level Sr/Ba trends.

Conclusion

This study of nineteen Early Islamic glass fragments from Jorjan demonstrates the predominance of plant-ash technology, with a balanced but variable contribution of Ca, K, and Na oxides. Grouping the assemblage into Na-poor, Na-moderate, and Na-rich categories reveals structured variability that reflects flexible workshop practices and multiple raw-material sources. Subtle enrichments in Sr and Ba further point to diverse sand inputs and underline the potential of isotopic and trace-element studies for provenance. The distribution of Fe, Mn, and Cu indicates deliberate use of colorants and decolorants, consistent with Early Islamic technological and aesthetic traditions. In regional perspective, the Jorjan assemblage aligns with findings from Rayy, Istakhr, and Bukhara, highlighting both shared technological frameworks and local adaptations within Silk Road exchange networks. Methodologically, the integration of LIBS for rapid, micro-destructive screening with SEM–EDS for calibrated quantification illustrates the strength of multi-method approaches in archaeometric research. Overall, the Jorjan glass exemplifies the technological dynamism of Early Islamic workshops, combining common traditions with local flexibility.

Data Availability

The data underlying the results presented in this paper are not publicly available at this time but may be obtained from the corresponding author upon reasonable request.

Conflict of Interest

The results obtained in this research do not conflict with any individual or organization.

Funding

This study did not receive any financial support.

Authors' Participation

This research is derived from the first author's doctoral dissertation. The primary data collection, encompassing all observational and analytical components, was conducted by the first author under the direct supervision and mentorship of the second, third, fourth and fifth authors.

References

Bayat Nejad, F., Emami, M., Eghbal Chehri, M., Kolbadinejad, M., & Chapoulie, R. (2025). Insights into late Sasanian glass workshop at the city of Istakhr, Fras; synchrotron XRF radiation techniques for glass characterization. Archaeometry. https://doi.org/10.1111/ARCM.13104

Brill, R. H. (1999). Chemical analyses of early glasses. Corning Museum of Glass.

Botto, A., Allegrini, F., Legnaioli, S., Lorenzetti, G., Pagnotta, S., & Palleschi, V. (2019). Applications of laser-induced breakdown spectroscopy in cultural heritage and archaeology: A critical review. Journal of Analytical Atomic Spectrometry, 34(1), 81–103. https://doi.org/10.1039/C8JA00328F

Detalle, V., et al. (2022). Laser-induced breakdown spectroscopy for cultural heritage: State of the art and future perspectives. Spectrochimica Acta Part B: Atomic Spectroscopy, 190, 106388. https://doi.org/10.1016/j.sab.2022.106388

Detalle, V., & Bai, X. (2022). The assets of laser induced breakdown spectroscopy (LIBS) for the future of heritage science. *Spectrochimica Acta Part B: Atomic Spectroscopy, 194*, 106–123.

De Sá, J. M. S., Pereira, M. F., Santos, D., & Alves, L. C. (2011). Applications of LIBS in archaeology: A review. *Journal of Archaeological Science, 38*(5), 983–992.

Degryse, P., & Schneider, J. (2008). Pliny the Elder and Sr–isotopes: Tracing the provenance of raw materials for Roman glass production. Journal of Archaeological Science, 35(7), 1993–2000.

Freestone, I. C. (2006). Glass production in Late Antiquity and the Early Islamic period. *Archaeometry, 48*(1), 35–57.

Kramida, A., Ralchenko, Y., Reader, J., & NIST ASD Team. (2024). *NIST Atomic Spectra Database* (Version 5.12). National Institute of Standards and Technology. https://physics.nist.gov/asd

Klein, S., Hildenhagen, J., Dickmann, K., Stratoudaki, T., & Zafiropulos, V. (2000). LIBS-spectroscopy for monitoring and control of the laser cleaning process of stone and medieval glass. Journal of Cultural Heritage, 1(Suppl. 1), S287–S292. https://doi.org/10.1016/S1296-2074(00)00177-4

Lü, Q.-Q., et al. (2023). Isotopic analysis refines provenance for Islamic plant ash glass in the eastern Islamic region. *iScience, 26*, Article e10758870.

May, R. A., et al. (2016). Characterization of ancient glass from the Roman Empire using laser induced breakdown spectroscopy. *Analytical Methods, 8*(12), 2510–2518.

Phelps, M., Freestone, I. C., Gorin Rosen, Y., & Gratuze, B. (2016). Natron glass production and supply in the Near East. *Journal of Archaeological Science, 75*, 57–71.

Paynter, S. (2008). Experiments in the reconstruction of Roman wood-fired glassworking furnaces: waste products and their formation processes. Journal of Archaeological Science, 35(9), 2576–2585.

Oujja, M., Palomar, T., Rodríguez, F. J., Herrero, M., Domingo, C., & Castillejo, M. (2021). Characterization of medieval-like glass alteration layers by complementary spectroscopy and microscopy techniques. The European Physical Journal Plus, 136(1), 859. https://doi.org/10.1140/epjp/s13360-021-01759-y

Rehren, T., & Freestone, I. C. (2015). Ancient glass: From kaleidoscope to crystal ball. Journal of Archaeological Science, 56, 233–241.

Schibille, N., Klesner, C., Neuville, D. R., Stark, S., & co authors. (2024). Geochemical variations in early Islamic glass finds from Bukhara (Uzbekistan). *Geochemistry*. Advance online publication.

Schibille, N., Lankton, J. W., & Gratuze, B. (2022). Compositions of early Islamic glass along the Iranian Silk Road. *Geochemistry, 82*, 125903.

Schibille, N., et al. (2018). Compositions of early Islamic glass along the Iranian Silk Road. *Journal of Archaeological Science, 97*, 48–63.

Schlatter, N., et al. (2024). Laser induced breakdown spectroscopy applied to cultural heritage: Recent advances and perspectives. *Heritage, 2*(1), 1–32.

Shortland, A. (2004). Natron as a flux in the early vitreous materials industry. *Archaeometry, 46*(1), 85–91.

Shortland, A., Schachner, L., Freestone, I., & Tite, M. (2006). Natron as a flux in the early vitreous materials industry: Sources, beginnings and reasons for decline. Journal of Archaeological Science, 33(4), 521–530.

Skrzeczanowski, W., et al. (2022). Application of laser-induced breakdown spectroscopy in the quantitative analysis of elements—K, Na, Ca, and Mg—in liquid solutions. Materials, 15(10), 3736. https://doi.org/10.3390/ma15103736

Schibille, N., Sterrett-Krause, A., & Freestone, I. C. (2018). Glass groups, glass supply and recycling in late Roman Carthage. Archaeological and Anthropological Sciences, 10(5), 1039–1056.

Van der Sloot, B., et al. (2007). LIBS for the analysis of archaeological glass: A non destructive tool for cultural heritage studies. *Applied Physics A, 89*(4), 953–959.